Performance assessment of the ITER ICRF antenna

F. Durodié, M. Vrancken, R. Bamber, L. Colas, P. Dumortier, D. Hancock, S. Huygen, D. Lockley, F. Louche, R.Maggiora, D. Milanesio, A. Messiaen, M. P. S. Nightingale, M. Shannon, P. Tigwell, M. Van Schoor, D. Wilson, K. Winkler, and CYCLE Team

Performance assessment of the ITER ICRF antenna

F. Durodié, M. Vrancken, R. Bamber, L. Colas, P. Dumortier, D. Hancock, S. Huygen, D. Lockley, F. Louche, R. Maggiora, D. Milanesio, A. Messiaen, M. P. S. Nightingale, M. Shannon, P. Tigwell, M. Van Schoor, D. Wilson, K. Winkler, and CYCLE Team

Citation: AIP Conference Proceedings **1580**, 362 (2014); doi: 10.1063/1.4864563
View online: http://dx.doi.org/10.1063/1.4864563
View Table of Contents: http://scitation.aip.org/content/aip/proceeding/aipcp/1580?ver=pdfcov
Published by the AIP Publishing

Performance Assessment of the ITER ICRF Antenna

F. Durodié[*], M. Vrancken[*], R. Bamber[†], L. Colas[**], P. Dumortier[*], D. Hancock[†], S. Huygen[*], D. Lockley[†], F. Louche[*], R. Maggiora[‡], D. Milanesio[‡], A. Messiaen[*], M.P.S. Nightingale[†], M. Shannon[†], P. Tigwell[†], M. Van Schoor[*], D. Wilson[†], K. Winkler[§] and CYCLE Team[¶]

[*]*LPP-ERM/KMS, Association EURATOM-Belgian State, Brussels, Belgium*
[†]*EURATOM/CCFE Association, Culham Science Centre, Abingdon, OX14 3DB, UK*
[**]*Association EURATOM-CEA, DSM/IRFM, Cadarache, France*
[‡]*Associazione EURATOM-ENEA, Politechnico di Torino, Italy*
[§]*IPP-MPI, EURATOM-Assoziation, Garching, Germany*
[¶]*(participating institutions above)*

Abstract. ITER's Ion Cyclotron Range of Frequencies (ICRF) system [1] comprises two antenna launchers designed by CYCLE (a consortium of European associations listed in the author affiliations above) on behalf F4E for the ITER Organisation (IO), each inserted as a Port Plug (PP) into one of ITER's Vacuum Vessel (VV) ports. Each launcher is an array of 4 toroidal by 6 poloidal RF current straps specified to couple up to 20 MW in total to the plasma in the frequency range of 40 to 55 MHz but limited to a maximum system voltage of 45 kV and limits on RF electric fields depending on their location and direction with respect to respectively the torus vacuum and the toroidal magnetic field. A crucial aspect of coupling ICRF power to plasmas is the knowledge of the plasma density profiles in the Scrape-Off Layer (SOL) and the location of the RF current straps with respect to the SOL. The launcher layout and details were optimized and its performance estimated for a worst case SOL provided by the IO. The paper summarizes the estimated performance obtained within the operational parameter space specified by IO. Aspects of the RF grounding of the whole antenna PP to the VV port and the effect of the voids between the PP and the Blanket Shielding Modules (BSM) surrounding the antenna front are discussed.

Keywords: ITER, ICRH, Launcher, Power
PACS: 52.50.Qt

INTRODUCTION

The design of the ITER ICRF launcher is supported by the results obtained with the ITER-Like Antenna on JET in 2008-9 [2] which validate the TOPICA [3] coupling estimations; demonstrate that there were no unforeseen difficulties in operating up to 42 kV (which was not a limit); achieved power densities in the range required by ITER in terms of reliability and did not result in excessive ICRF impurity production. Additional confirmation of the proposed matching and its load resilient operation were also demonstrated on ELMy plasmas on JET's A2 ICRF antennas [4, 5]. *FIG. 1* shows a poloidal section of 1 of 8 similar sub-assemblies arranged in a 2 poloidal by 4 toroidal array making up the whole array and its CST Microwave Studio [6] 3D RF model where the outer conductors have been left out.

RF OPTIMIZATION AND ESTIMATED PERFORMANCE

ITER ICRF antenna's capability to couple power to plasma is determined by : the plasma SOL location and profiles [7]; the shaping of the front strap array, organized as a 6 poloidal by 4 toroidal array of short straps; the overall layout of the feed network and the detailed design of its RF components. The first two factors are taken into account in the strap array 24x24 scattering or impedance matrices, S_{24} resp. Z_{24}, calculated by TOPICA [3] by importing a CAD model of front face of the antenna and using plasma Scrape-Off Layer (SOL) profiles given by ITER Organization (IO) [8] depending on the physics assumptions used for modelling ITER's SOL. The "Low density SOL" case results in lower coupling than pre-project assumptions [9] while the "High density SOL" case is particularly favourable to couple ICRH power but may not be feasible due to the heat loads on ITER's First Wall (FW). The S_{24}/Z_{24} matrix data is coupled to a RF circuit model of the circuit feeding the straps of which the components are represented by either S or Z matrices estimated with CST Microwave Studio, such as the 4 Port Junction (4PJ) feeding 3 poloidally adjacent straps, or simple Transmission Line (TL) sections for the rest of the Removable Vacuum Transmission Line (RVTL) which include the Service Stub tee (SS-T) and Vacuum Ceramic Windows (VCW). The accuracy of joining the strap array 24x24 matrices from TOPICA to the S-matrix RF model of the 4PJ was verified and the effects of the presence of non-TEM modes in the plane of the connection between 4PJ and strap feeders appear to be minimal.

The circuit components inside the port plug are optimized to maximize the power coupled to the plasma for the various phasings considered for operation taking into account geometrical constraints, assembly requirements and RF quantities specified by IO: E-field less than 2 kV/mm parallel to the magnetic field in the torus vacuum areas and

Radiofrequency Power in Plasmas
AIP Conf. Proc. 1580, 362-365 (2014); doi: 10.1063/1.4864563
2014 AIP Publishing LLC 978-0-7354-1210-1/$30.00

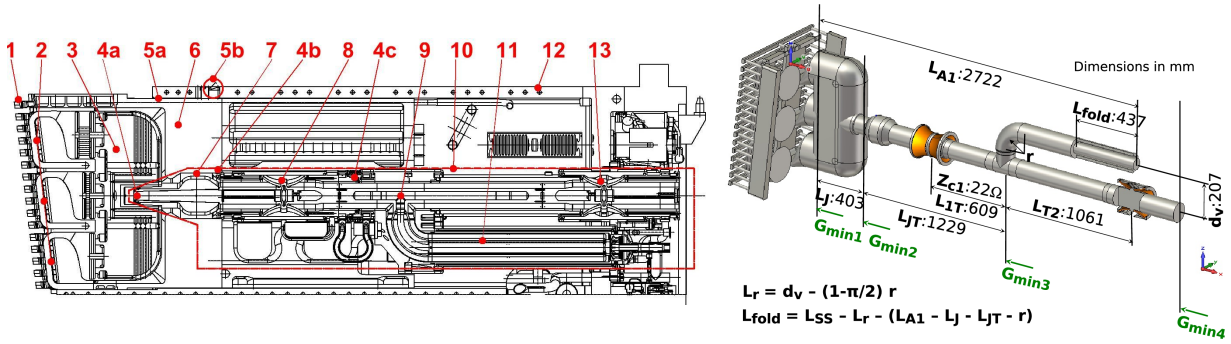

FIGURE 1. (left) Section through of 1 of the 8 triplets of straps and feeding RVTL: (1) Faraday Screen, (2) RF current straps, (3) 4PJ, (4) RVTL RF contacts (a,b) resp. inner and outer conductors for assembly and shimming, (c) outer conductor for thermal expansion, (5) RF contacts (a) FHM-PP grounding for assembly and shimming, (b) deployable PP-VV grounding contact, (6) FHM, (7) direct line of sight neutron shield for the (8) 1st VCW, (9) SS-T, (10) RVTL, (11) SS, (12) PP, (13) rear VCW. (right) Schematic CST-MWS RF model layout showing the inner conductors of 1 of 8 similar triplets, 4PJ, VCWs (ceramics cones shown at the beginning and end of sections L_{1T} and L_{2T}), SS and RVTL assemblies and parameters used for optimizing the performance.

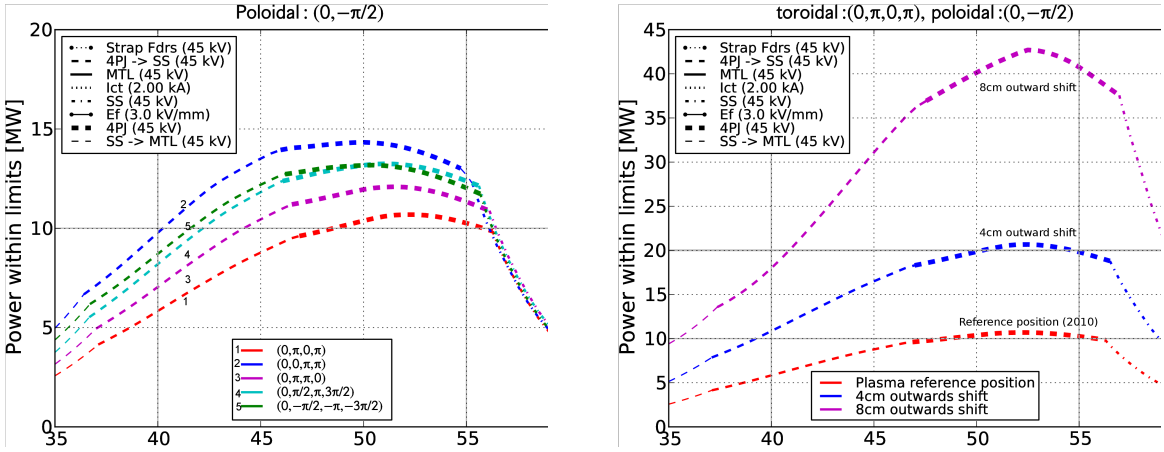

FIGURE 2. (left) resulting estimate of coupled power for the various toroidal phasings for the reference poloidal phasing $(0,-\pi/2)$, (right) performance for the $(0,\pi,0,\pi)$ toroidal phasing and $(0,-\pi/2)$ poloidal phasing for SOL profiles shifted towards the antenna.

magnitude less than 3 kV/mm everywhere and voltages less than 45 kV. Additionally, the CYCLE team has specified, subject to a successful outcome of related R&D [10], currents less than 2 kA through RF contact with the highest current density (5 kA/m) between RVTL and 4PJ inner conductors. The arrows indicating the positions $G_{min,k}$ on *FIG. 1 (right)* delimit the various sections where the circuit simulator verifies that the aforementioned electrical limits are not exceeded [9, 11] (formally $G_{min,k}$ refers to the minimum conductance and the power launched for 1 triplet is given by $P_{RF,k} = 0.5 \times G_{min,k} \times V^2_{max,k}$ for maximum voltage $V_{max,k}$ on an extended homogeneous TL longer than half wavelength feeding the resp. section k (k = 1: antenna strap feeders, 2: 4PJ to the SS-tee, 3: SS-tee to the feeding MTL excluding 2^{nd} VCW, 4: feeding MTL past the 2^{nd} VCW)). However, the circuit solver further takes into account (a) an estimate of the voltage distribution on the 4PJ, (b) that the maximum voltages do not always appear on the sections that are shorter than half a wavelength (allowing the transmitted power to increase if not limited elsewhere), (c) that the current density in the RF contact between 4PJ and RVTL inner conductor, I_{ct} and (d) the electric field at the inward fold of the SS, E_f remain within allowed limits. *FIG. 2 (left)* shows how the power coupled to the plasma is limited by the RF quantities in the various sections and locations for the toroidal phasing of $(0,\pi,0,\pi)$ and the reference poloidal phasing $(0,-\pi/2)$. The resulting overall performance curve for this phasing is then the minimum over all curves and is shown in *FIG. 2 (right)* together with similar curves for other toroidal phasings. The maximum E-field on the components is limited by shaping their surface such that the design limits are not exceeded either at the maximum system voltage of 45 kV (4PJ, RVTL, VCW, SS) or at the maximum expected voltage (SS fold region). The optimisation is most sensitive to the length of the 4PJ (L_J) for which an accuracy of $< 10mm$ must be achieved : if the 4PJ is too long the cliff-edge like limitation due to the RF contact current shifts downwards from the high frequency side and if it is too short the performance at the low frequencies is further degraded. For the other

dimensional parameters the sensitivity is not as severe. The optimisation of the layout in terms of the parameters shown in *FIG. 1 (right)* is not unique [12]: the solution presented in this paper uses two identical VCW assemblies with a slightly higher average characteristic impedance (to depart as little as possible of the optimal mechanical design of the VCW [13, 14]) than that of the RVTL (20 Ω) at the cost of a slightly reduced performance at the high frequencies as well as reduction by about 0.3 MHz of the margin to the cliff-edge like limitations at high frequency. The performance of the launcher is unsurprisingly very sensitive to the location of the SOL plasma profile in front of the antenna straps. *FIG. 2 (right)* shows the power coupled to the plasma for profiles shifted (in an ad hoc manner in the input to the TOPICA coupling code) by 4 and 8 cm towards the antenna with respect to the reference position. It has been suggested by IO [15] that it should be possible to shift the plasma closer to the antenna while the heat load on the FW remains acceptable. Recently a consistent plasma equilibrium has been received from IO [16] that amounts to a shift of the SOL profile towards the antenna by more than 10 cm. The compatibility with respect to the FW still needs to be assessed. Finally, the performance can be improved by about 20% by feeding the array poloidaly in $(0, \pi)$ phasing rather than $(0, -\pi/2)$. [17] proposes a modification of the matching network to achieve this for toroidal current drive phasings. Losses are highest at high frequency with a minimum at mid-band frequency and amount to a maximum of 1.12 MW for the whole launcher at 55 MHz [12].

RF MEASUREMENTS AND CONTROL ASPECTS

Redundant RF measurements are necessary to control the launched power spectrum, to operate the antenna within prescribed limits with confidence and to protect the launcher in case of arcs. Each RVTL asssembly is fitted with two pairs of RF probes that each measure local voltage as well as current simultaneously [18]. These probes can also been used for Arc Detection although analysis shows that arcs located where the RF voltage of the Voltage Standing Wave (VSW) is low are not detected [18]. This a problem common to most arc detection techniques based on RF signals so that other methods should be used additionally [19, 20]. The estimates of performance shown assume that the control of the RF power feeding the strap array will be done using RF measurements of the amplitude and phase of the RF voltages located at the average position of the voltage anti-nodes on the 8 feeding main TLs [9]. The main effect is that even with error free measurements the errors on the strap current amplitude and phases will be substantially larger than for the ideal (but possibly not feasible) control which mathematically minimizes the strap current amplitude and phase errors [21]. Note that because there are 24 straps and only 8 feeding TLs and the presence of asymmetries due to e.g. the non-reciprocity of the plasma, the strap current amplitude and phase errors cannot be zeroed even in the case of an ideal control. These errors become larger when the coupling with the plasma is increased and when the phasing (poloidal as well as toroidal) leads to RF power transfers ($\pi/2$ phase differences between adjacent triplets). These amplitude and phase errors may in turn increase RF sheath losses on the Antenna's Faraday Screen (FS) and adjacent BSM. Although progress has been made in the modelling of the physics of RF sheath in tokamak environments [22, 23] the problem remains computationally complex, still necessitating geometric as well as physics simplifications such that a sufficiently accurate quantification of the RF power dissipated in the RF sheaths is still outstanding. In order to cope with these uncertainties the position of the launcher with respect to the plasma can be varied during shutdowns : it can be moved 1cm towards the plasma to improve the coupling should it be too marginal and 2cm away from the plasma should RF sheaths and other heat loads on the FS bars exceed their thermal capabilities.

GROUNDING

Theoretical and experimental [24, 25] efforts were spent to understand the aspects of the grounding of the PP to the VV to avoid spurious resonances in the 24x24 strap impedance matrix [26] as well as the presence of high electric fields in the nominal 20mm gap between the PP and VV [27]. The effectiveness of the proposed grounding to reduce electric fields in these areas is discussed in [28] which shows that without the additional grounding towards the front of the PP the fields can even exceed these on the high power components of the launcher. The possible appearance of resonances on the coupled power vs. frequency curves are due to the presence of gaps of varying widths between the front of the launcher and the surrounding Blanket Shielding Modules (BSM) [26].

However, it is stretching present capabilities to RF model realistically the real geometry of the objects around the front of the antenna filling these gaps, such as cooling pipes and ELM stabilization coils and their intermittent grounding and attachment to the VV, to totally exclude the presence of similar resonances. The CYCLE team has proposed to develop and test on scaled mock-ups of the launcher [29] low power measurement procedures on the installed port plug to detect possible resonances and avoid operating at these frequencies if detected.

CONCLUSIONS

The proposed layout for the ITER ICRF launcher has been optimized to maximize the coupled power on the worst case plasma SOL profile provided by IO. It is expected that at least 10 MW/launcher can be coupled to the plasma at frequencies above the mid-band frequency for all toroidal phasings and a poloidal phasing of $(0, -\pi/2)$. The location of the plasma SOL is a very sensitive parameter and it is very likely that the situation can be improved substantially. The sensitivity of the optimisation to the dimensional parameters appears to be mechanically reasonable and on the order of about 10mm for the most sensitive component. Particular attention has been given to the RF grounding aspects of the launcher to avoid spurious resonances and high electric fields in the gap between the PP and the VV port.

ACKNOWLEDGMENTS

The project F4E-2009-GRT-026 has been funded by the Consortium members with support from Fusion for Energy. This publication reflects the views only of the author, and Fusion for Energy cannot be held responsible for any use which may be made of the information contained herein. The views and opinions expressed herein do not necessarily reflect those of the ITER Organization.

REFERENCES

1. P. Lamalle *et al.*, "Status of the ITER Ion Cyclotron H & CD system," in *24th SOFT, Liège (Belgium)*, 2012.
2. F. Durodié *et al.*, *Pl. Phys. and Contr. Fus.* **54** (2012), http://dx.doi.org/10.1088/0741-3335/54/7/074012.
3. V. Lancellotti *et al.*, *Nuclear Fusion* **46**, S476 – S499 (2006).
4. M. Graham *et al.*, *Pl. Phys. and Contr. Fus.* **54** (2012), http://dx.doi.org/10.1088/0741-3335/54/7/074011.
5. I. Monakhov *et al.*, Design and operations of load-tolerant external conjugate-T matching system for the A2 ICRH antennas at JET (2012), to be submitted to Nuclear Fusion.
6. *CST Microwave Studio®, User Manual*, CST GmbH (2011).
7. A. Messiaen, and R. Weynants, *Plasma Physics and Controlled Fusion* **53** (2011), http://dx.doi.org/10.1088/0741-3335/53/8/085020.
8. S. Carpentier-Chouchana *et al.*, *J. Nucl. Mat.* **415**, S165 – S169 (2011), http://dx.doi.org/10.1016/j.jnucmat.2010.10.081.
9. A. Messiaen *et al.*, *Nuclear Fusion* **50** (2010), http://dx.doi.org/10.1088/0029-5515/50/2/025026.
10. A. Argouarch *et al.*, "Steady State RF Facility for Testing ITER ICRH RF Contact Component," in *Procedings of the 24th SOFT, Liège (Belgium)*, 2012.
11. P. Dumortier *et al.*, "Validation of the RF Properties and Control of the ITER ICRF Antenna," in *Proceedings of 24th IAEA Fusion Energy Conference 2012, San Diego (US)*, 2012.
12. M. Vrancken *et al.*, "RF Optimisation of the Port Plug Layout and Performance Assessment of the ITER ICRF Antenna," in *24th SOFT, Liège (Belgium)*, 2012.
13. C. Hamlyn-Harris *et al.*, *Fusion Engineering and Design* **84**, 887–894 (2009), http://dx.doi.org/10.1016/j.fusengdes.2008.12.124.
14. R. Walton, A Continuous Wave RF Vacuum Window (1999), JET Report JET-R(99)03.
15. A. Loarte (2010), private communication.
16. S. Carpentier-Chouchana, New dens. prof. for ICRH - 'pulled out' equilibr. - Aug. 2012.xls (2012), per e-mail via P. Lamalle.
17. M. Vervier *et al.*, "Technical Optimization of the ITER ICRH Decoupling and Matching System," in *24th SOFT, Liège (Belgium)*, 2012.
18. S. Huygen *et al.*, "Proposal of an Arc Detection Technique Based on RF Measurements for the ITER ICRF Antenna," in *AIP Conf. Proc. 1406 (2011)*, 2011, pp. 21–24, http://dx.doi.org/10.1063/1.3664920.
19. R. D'Inca, "Arc detection for the ICRF system on ITER," in *AIP Conf. Proc. 1406 (2011)*, 2011, pp. 5–12, http://dx.doi.org/10.1063/1.3664917.
20. S. Salvador *et al.*, "Arc Detection With GUIDAR : First Experimental Tests On MXP Testbed," in *AIP Conf. Proc. 1406 (2011)*, 2011, pp. 25–28, http://dx.doi.org/10.1063/1.3664921.
21. M. Vrancken *et al.*, "Optimization of the Layout of the ITER ICRF Antenna Port Plug and its Performance Assessment," in *AIP Conf. Proc. 1406 (2011)*, 2011, pp. 61–64, http://dx.doi.org/10.1063/1.3664929.
22. L.Colas *et al.*, *Phys. Plasmas* **19** (2012), http://dx.doi.org/10.1063/1.4750046.
23. J. Jacquot *et al.*, "Recent advances in self-consistent RF sheath modeling and related physical properties: Application to Tore Supra IC antennae," in *39th EPS Conference & 16th Int. Congress on Plasma Physics*, 2012, http://ocs.ciemat.es/EPSICPP2012PAP/pdf/P2.038.pdf.
24. P. Dumortier *et al.*, "ITER ICRH Antenna Grounding Options," in *Procedings of the 24th SOFT, Liège (Belgium)*, 2012.
25. D. Hancock *et al.*, "Grounding Aspects of the ICRF Antenna for ITER," in *24th SOFT, Liège (Belgium)*, 2012.
26. F. Louche *et al.*, "Influence of the Blanket Shield Modules Geometry on the Operation of the ITER ICRF Antenna," in *24th SOFT, Liège (Belgium)*, 2012.
27. F. Louche *et al.*, *Nuclear Fusion* **49** (2009), http://dx.doi.org/10.1088/0029-5515/49/6/065025.
28. F. Louche, and V. Kyrytsya, CIA Report on Coupling and Grounding (2012), private communication.
29. P. Dumortier *et al.*, "Validation of the Electrical Properties of the ITER ICRF Antenna using Reduced-Scale Mock-Ups," in *AIP Conf. Proc. 1406 (2011)*, 2011, pp. 29–36, http://dx.doi.org/10.1063/1.3664922.